Inorganic Chemistry
Article

Inorg. Chem. **2011**, *50*, 1459–1469 **1459**
DOI: 10.1021/ic102016k

$(N_2)^{3-}$ Radical Chemistry via Trivalent Lanthanide Salt/Alkali Metal Reduction of Dinitrogen: New Syntheses and Examples of $(N_2)^{2-}$ and $(N_2)^{3-}$ Complexes and Density Functional Theory Comparisons of Closed Shell Sc^{3+}, Y^{3+}, and Lu^{3+} versus $4f^9$ Dy^{3+}

Ming Fang, Jefferson E. Bates, Sara E. Lorenz, David S. Lee, Daniel B. Rego, Joseph W. Ziller, Filipp Furche, and William J. Evans*

Department of Chemistry, University of California, Irvine, California 92697-2025, United States

Received October 4, 2010

New syntheses of complexes containing the recently discovered $(N_2)^{3-}$ radical trianion have been developed by examining variations on the LnA_3/M reductive system that delivers "LnA_2" reactivity when Ln = scandium, yttrium, or a lanthanide, M = an alkali metal, and A = $N(SiMe_3)_2$ and C_5R_5. The first examples of LnA_3/M reduction of dinitrogen with aryloxide ligands (A = OC_6R_5) are reported: the combination of $Dy(OAr)_3$ (OAr = $OC_6H_3{}^tBu_2$-2,6) with KC_8 under dinitrogen was found to produce both $(N_2)^{2-}$ and $(N_2)^{3-}$ products, $[(ArO)_2Dy(THF)_2]_2(\mu\text{-}\eta^2\text{:}\eta^2\text{-}N_2)$, **1**, and $[(ArO)_2Dy(THF)]_2(\mu\text{-}\eta^2\text{:}\eta^2\text{-}N_2)[K(THF)_6]$, **2a**, respectively. The range of metals that form $(N_2)^{3-}$ complexes with $[N(SiMe_3)_2]^-$ ancillary ligands has been expanded from Y to Lu, Er, and La. $Ln[N(SiMe_3)_2]_3$/M reactions with M = Na as well as KC_8 are reported. Reduction of the isolated $(N_2)^{2-}$ complex $\{[(Me_3Si)_2N]_2Y(THF)\}_2(\mu\text{-}\eta^2\text{:}\eta^2\text{-}N_2)$, **3**, with KC_8 forms the $(N_2)^{3-}$ complex, $\{[(Me_3Si)_2N]_2Y(THF)\}_2(\mu\text{-}\eta^2\text{:}\eta^2\text{-}N_2)[K(THF)_6]$, **4a**, in high yield. The reverse transformation, the conversion of **4a** to **3** can be accomplished cleanly with elemental Hg. The crown ether derivative $\{[(Me_3Si)_2N]_2Y(THF)\}_2(\mu\text{-}\eta^2\text{:}\eta^2\text{-}N_2)[K(18\text{-crown-}6)(THF)_2]$ was isolated from reduction of **3** with KC_8 in the presence of 18-crown-6 and found to be much less soluble in tetrahydrofuran (THF) than the $[K(THF)_6]^+$ salt, which facilitates its separation from **3**. Evidence for ligand metalation in the $Y[N(SiMe_3)_2]_3/KC_8$ reaction was obtained through the crystal structure of the metallacyclic complex $\{[(Me_3Si)_2N]_2Y[CH_2Si(Me_2)NSiMe_3]\}[K(18\text{-crown-}6)(THF)(toluene)]$. Density functional theory previously used only with reduced dinitrogen complexes of closed shell Sc^{3+} and Y^{3+} was extended to Lu^{3+} as well as to open shell $4f^9$ Dy^{3+} complexes to allow the first comparison of bonding between these four metals.

Introduction

The $(N_2)^{3-}$ radical was recently synthesized for the first time in complexes of dysprosium and yttrium, Schemes 1 and 2.[1] Although $(N_2)^{3-}$ is isoelectronic with the well-known $(O_2)^-$ superoxide ion[2] and dinitrogen reduction has been heavily studied,[3−15] this oxidation level of reduced dinitrogen had remained elusive for decades. Density functional theory (DFT) studies on the complex of the closed shell Y^{3+} ion indicated that the unpaired spin density in the $(N_2)^{3-}$ radical was located in an orbital perpendicular to the metal orbitals and the isolation of this reactive species may be facilitated by the ionic nature of Dy^{3+} and Y^{3+}.[1]

We report here on the expansion of $(N_2)^{3-}$ chemistry beyond the examples in Schemes 1 and 2 in terms of the lanthanide metals, alkali metals, ancillary ligands, and synthetic methods. Since these new developments were pursued to answer questions raised during the initial discovery of the $(N_2)^{3-}$ complexes, it is pertinent to review that chemistry here.

The first observation of an $(N_2)^{3-}$ ion arose from reduction of dinitrogen by a Ln^{2+} ion, specifically from the combination

*To whom correspondence should be addressed. E-mail: wevans@uci.edu.

(1) Evans, W. J.; Fang, M.; Zucchi, G.; Furche, F.; Ziller, J. W.; Hoekstra, R. M.; Zink, J. I. *J. Am. Chem. Soc.* **2009**, *131*, 11195.
(2) Kaim, W.; Sarkar, B. *Angew. Chem., Int. Ed.* **2009**, *48*, 9409.
(3) MacKay, B. A.; Fryzuk, M. D. *Chem. Rev.* **2004**, *104*, 385.
(4) Hidai, M. *Coord. Chem. Rev.* **1999**, *185−186*, 99.
(5) Gambarotta, S.; Scott, J. *Angew. Chem., Int. Ed.* **2004**, *43*, 5298.
(6) Holland, P. L. *Can. J. Chem.* **2005**, *83*, 296.
(7) Evans, W. J.; Lee, D. S. *Can. J. Chem.* **2005**, *83*, 375.
(8) Chirik, P. J. *Dalton Trans.* **2007**, 16.
(9) Schrock, R. R. *Angew. Chem., Int. Ed.* **2008**, *47*, 5512.
(10) Fryzuk, M. D. *Acc. Chem. Res.* **2009**, *42*, 127.
(11) Caselli, A.; Solari, E.; Scopelliti, R.; Floriani, C.; Re, N.; Rizzoli, C.; Chiesi-Villa, A. *J. Am. Chem. Soc.* **2000**, *122*, 3652.
(12) Curley, J. J.; Cook, T. R.; Reece, S. Y.; Müller, P.; Cummins, C. C. *J. Am. Chem. Soc.* **2008**, *130*, 9394.
(13) Jaroschik, F.; Momin, A.; Nief, F.; Goff, X.-F. L.; Deacon, G. B.; Junk, P. C. *Angew. Chem., Int. Ed.* **2009**, *48*, 1117.
(14) Fontaine, P. P.; Yonke, B. L.; Zavalij, P. Y.; Sita, L. R. *J. Am. Chem. Soc.* **2010**, *132*, 12273.
(15) Lee, Y.; Mankad, N. P.; Peters, J. C. *Nat. Chem.* **2010**, *2*, 558.

Published on Web 01/04/2011

Scheme 1. First $(N_2)^{3-}$ Complexes from DyI_2/KOAr Reduction of Dinitrogen (OAr = $OC_6H_3{}^tBu_2$-2,6)

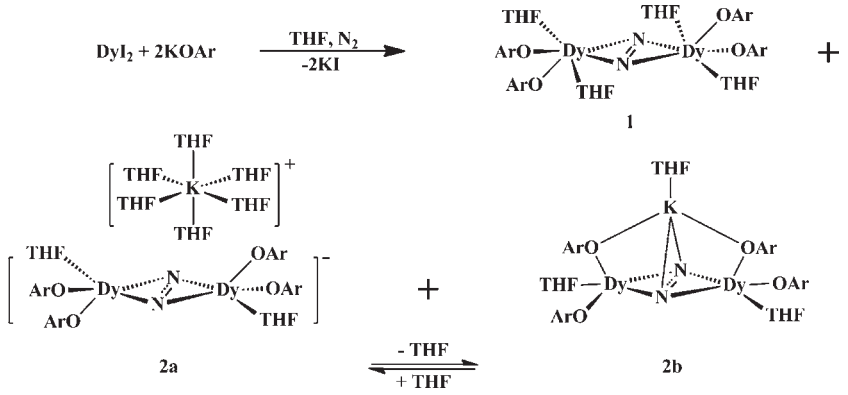

Scheme 2. $(N_2)^{3-}$ Complexes from the LnA_3/M Reductive System with Ln = Y, A = $N(SiMe_3)_2$, and M = KC_8

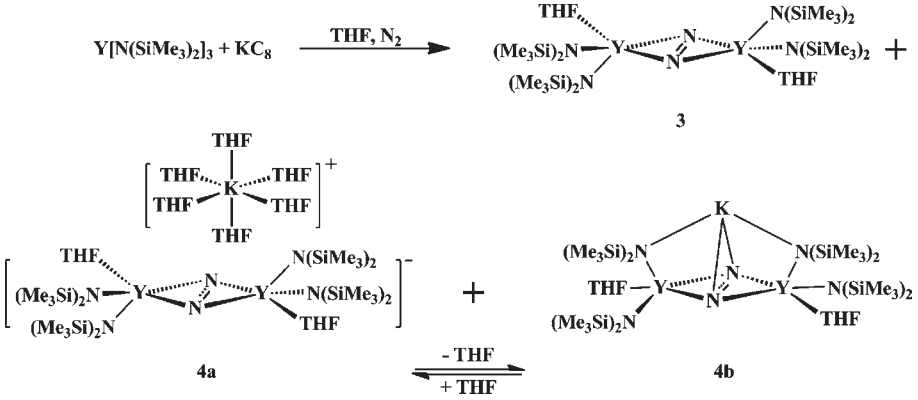

of DyI_2 and an aryloxide reagent, KOAr (OAr = $OC_6H_3{}^tBu_2$-2,6), as shown in Scheme 1. This reaction provided an $(N_2)^{2-}$ complex, $[(ArO)_2Dy(THF)_2]_2(\mu\text{-}\eta^2\text{:}\eta^2\text{-}N_2)$, **1**, as well as two $(N_2)^{3-}$ products, $[(ArO)_2Dy(THF)]_2(\mu\text{-}\eta^2\text{:}\eta^2\text{-}N_2)[K(THF)_6]$, **2a**, and $[(ArO)_2Dy(THF)]_2(\mu_3\text{-}\eta^2\text{:}\eta^2\text{:}\eta^2\text{-}N_2)K(THF)$, **2b**, that could be interconverted by addition or removal of tetrahydrofuran (THF). Because of the paramagnetism of the $4f^9$ Dy^{3+} products, confirmation of the existence of the $(N_2)^{3-}$ radical in **2a** and **2b** by electron paramagnetic resonance (EPR) spectroscopy or magnetic methods was not possible. Diamagnetic analogues of **2a** and **2b** with La, Y, or Lu would have provided definitive evidence, but the necessary Ln^{2+} precursors were not known for these metals. An alternative route to diamagnetic analogues of **2a** and **2b** involved accessing Ln^{2+} reactivity via the LnA_3/M method, formerly designated as the LnZ_3/M method[16] in which Ln is scandium, yttrium, or a lanthanide, M is an alkali metal, and A is a group that exists as an anion in LnA_3 and provides reductive reactivity in combination with an alkali metal or the equivalent. However, "LnA_2" reactivity had never been demonstrated in this way with aryloxide ligands, that is, A = OC_6R_5. The only A ligands that allowed LnA_3/M combinations to provide "LnA_2" reactivity were $N(SiMe_3)_2$ and C_5R_5 cyclopentadienyl ligands. We now describe the formation of both $(N_2)^{2-}$ and $(N_2)^{3-}$ complexes via $Dy(OAr)_3$/KC_8 reduction as well as attempts to expand this to diamagnetic metals.

Ultimately, the existence of the $(N_2)^{3-}$ ion was demonstrated by detailed investigations of the reduction of dinitrogen via the LnA_3/M reductive method with Ln = Y, A = $N(SiMe_3)_2$, and M = KC_8, Scheme 2. This $Y[N(SiMe_3)_2]_3/KC_8$ reaction had initially yielded the $(N_2)^{2-}$ product, $\{[(Me_3Si)_2N]_2Y(THF)\}_2(\mu\text{-}\eta^2\text{:}\eta^2\text{-}N_2)$, **3**, since it is the least soluble, most readily isolable component in the reaction mixture.[19] We now report that other LnA_3/M reactions that make $(N_2)^{2-}$ species as the major product[19,20] also form $(N_2)^{3-}$ complexes with $N(SiMe_3)_2$ ligands and Ln = Lu, Er, and La. In addition, we describe the first $(N_2)^{3-}$ complex with Na^+ as a countercation, a new route to $(N_2)^{3-}$ complexes using one-electron reduction of the $(N_2)^{2-}$ complexes, and the utility of 18-crown-6 in separating mixtures of $(N_2)^{2-}$ and $(N_2)^{3-}$ complexes. The implications of these results on the LnA_3/M reductive method and the formation of $(N_2)^{2-}$ and $(N_2)^{3-}$ ions in general are also presented.

In addition, we report DFT calculations on Lu^{3+} and Dy^{3+} complexes. Previously, DFT has been used to examine reduced dinitrogen complexes of only $3d^0$ Sc^{3+}[24] and $4d^0$ Y^{3+}[1] ions that

(16) A referee has pointed out that Z has been previously defined[17,18] as a ligand that accepts electrons in a dative bond from the metal like a BR_3 group. To avoid confusion, we will change the LnZ_3/M notation used in the past[1,7,19–24] to LnA_3/M where A is defined as a group that exists as an anion in LnA_3 and provides reductive reactivity in combination with an alkali metal or the equivalent.

(17) Green, M. L. H. *J. Organomet. Chem.* **1995**, *500*, 127.
(18) Sircoglou, M.; Bontemps, S.; Mercy, M.; Saffon, N.; Takahashi, M.; Bouhadir, G.; Maron, L.; Bourissou, D. *Angew. Chem., Int. Ed.* **2007**, *46*, 8583.
(19) Evans, W. J.; Lee, D. S.; Ziller, J. W. *J. Am. Chem. Soc.* **2004**, *126*, 454.
(20) Evans, W. J.; Lee, D. S.; Rego, D. B.; Perotti, J. M.; Kozimor, S. A.; Moore, E. K.; Ziller, J. W. *J. Am. Chem. Soc.* **2004**, *126*, 14574.
(21) Evans, W. J.; Lee, D. S.; Lie, C.; Ziller, J. W. *Angew. Chem., Int. Ed.* **2004**, *43*, 5517.
(22) Evans, W. J.; Lee, D. S.; Johnston, M. A.; Ziller, J. W. *Organometallics* **2005**, *24*, 6393.
(23) Evans, W. J.; Rego, D. B.; Ziller, J. W. *Inorg. Chem.* **2006**, *45*, 10790.
(24) Demir, S.; Lorenz, S. E.; Fang, M.; Furche, F.; Meyer, G.; Ziller, J. W.; Evans, W. J. *J. Am. Chem. Soc.* **2010**, *132*, 11151.

behave like lanthanides, but have no 4f valence orbitals or electrons. In this study, calculations on the closed shell $4f^{14}$ Lu^{3+} were performed to allow comparisons with Sc^{3+} and Y^{3+}. We also report converged calculations on the open shell $4f^{9}$ Dy^{3+}. This provides the first comprehensive comparison of a series of scandium, yttrium, lutetium, and open shell lanthanide ions.

Experimental Section

The syntheses and manipulations described below were conducted under argon or nitrogen with rigorous exclusion of air and water using glovebox, vacuum line, and Schlenk techniques. Potassium and sodium were purchased from Aldrich, washed with hexanes, and scraped to provide fresh surfaces before use. $HOC_6H_3{}^tBu_2$-2,6 (ArOH) and 18-crown-6 were purchased from Aldrich and sublimed prior to use. Solvents were dried over columns containing Q-5 and molecular sieves. NMR solvents were dried over sodium−potassium alloy, degassed using three freeze−pump−thaw cycles, and vacuum transferred prior to use. Potassium bis(trimethylsilyl)amide (Aldrich) was dissolved in toluene, and the mixture was centrifuged and decanted to remove tacky yellow insoluble material before use. Regeneration gas (10% H_2 in N_2) was purchased from Airgas and used without further purification. $^{15}N_2$ (> 98%) was purchased from Cambridge Isotope Laboratories and used without further purification. KC_8[25] and the $Ln[N(SiMe_3)_2]_3$ complexes (Ln = Y, Lu, Er, Dy, and La)[26] were prepared according to literature methods. $Dy(OAr)_3$ (OAr = $OC_6H_3{}^tBu_2$-2,6) was prepared by protonolysis of $Dy[N(SiMe_3)_2]_3$ with ArOH.[27] $\{[(Me_3Si)_2N]_2Y(THF)\}_2(\mu\text{-}\eta^2\text{:}\eta^2\text{-}N_2)$, **3**, was synthesized via LnA_3/KC_8 methods.[19,20] ^1H and ^{13}C NMR spectra were obtained on a Bruker DRX500 MHz spectrometer at 25 °C. EPR spectra were collected using a Bruker EMX spectrometer equipped with an ER041XG microwave bridge. The magnetic field was calibrated with DPPH, and all experiments were done at room temperature. SIMPOW6[28] developed by Professor Nilges at the University of Illinois was used to simulate the EPR spectra. IR samples were prepared as KBr pellets, and the spectra were obtained on a Varian 1000 FT-IR system. Elemental analyses were performed on a PerkinElmer Series II 2400 CHNS elemental analyzer.

$[(ArO)_2Dy(THF)_2]_2(\mu\text{-}\eta^2\text{:}\eta^2\text{-}N_2)$, 1, and $[(ArO)_2Dy(THF)]_2(\mu\text{-}\eta^2\text{:}\eta^2\text{-}N_2)[K(THF)_6]$, 2a. In a nitrogen-filled glovebox, a colorless solution of $Dy(OAr)_3$ (250 mg, 0.32 mmol) in 30 mL of THF was added to a 100 mL round-bottom flask containing KC_8 (65 mg, 0.48 mmol) and a stirbar. The reaction immediately turned dark brown. After 2 h, the reaction mixture was centrifuged to remove the insoluble material, and the solvent was evaporated under vacuum. The oily yellow-brown residue was extracted with 25 mL of toluene, separated from the insoluble material, and concentrated. Over the course of 2 d at −35 °C, X-ray quality crystals of **1** (47 mg, 20%) were isolated. The toluene insoluble material was dissolved in THF, concentrated, and crystallized at −35 °C over the course of 3 d to yield brown X-ray quality crystals of **2a** (83 mg, 29%).

$\{[(Me_3Si)_2N]_2Lu(THF)\}_2(\mu\text{-}\eta^2\text{:}\eta^2\text{-}N_2)[K(THF)_6]$, 6. In a nitrogen-filled glovebox, KC_8 (0.330 g, 2.44 mmol) was slowly added over 20 min at ambient temperature to a stirred solution of $Lu[N(SiMe_3)_2]_3$ (1.60 g, 2.44 mmol) in 80 mL of THF. The resulting brown suspension was allowed to stir for an additional 30 min. The reaction mixture was centrifuged and filtered to remove dark insoluble material, presumably graphite, and evaporation of the filtrate yielded a yellow tacky solid. The yellow solid was dissolved in 5 mL of THF and stored at −35 °C to produce **6** (0.40 g, 20%) as yellow-orange crystals after 2 d. IR: 2948 m, 2895 m, 2470w, 2347w, 2085w, 1911w, 1852w, 1578w, 1437 m, 1400 m, 1246s, 1183w, 1053sh, 967s, 866s, 831s, 776 m, 752 m, 702w, 666 m, 612 m cm^{-1}. Examination of the yellow orange mother liquor by ^1H NMR spectroscopy revealed that $\{[(Me_3Si)_2N]_2Lu(THF)\}_2(\mu\text{-}\eta^2\text{:}\eta^2\text{-}N_2)$, **5**, previously isolated from this system when a THF solution of $Lu[N(SiMe_3)_2]_3$ was quickly added to KC_8,[19] was present as a byproduct. Since compound **5** is much less soluble in THF than paramagnetic **6**, it was expected that **5** would crystallize out of the THF solution first if it were present in a larger amount than **6**. The fact that **6** was the first to precipitate from the THF solution showed that the slow addition method reported here favors **6**.

$\{[(Me_3Si)_2N]_2La(THF)_x\}_2(\mu\text{-}\eta^2\text{:}\eta^2\text{-}N_2)[K(THF)_y]$, 7. In a nitrogen-filled glovebox, KC_8 (22 mg, 0.16 mmol) was slowly added over 2 min at ambient temperature to a stirred solution of $La[N(SiMe_3)_2]_3$ (100 mg, 0.16 mmol) in 10 mL of THF. The solution immediately became brown and was allowed to stir for an additional 10 min. The reaction mixture was centrifuged and filtered to remove dark insoluble material, presumably graphite, and evaporation of the filtrate yielded a tacky yellow solid. Crystallization of this tacky solid in about 1 mL of THF at −35 °C afforded colorless crystals which were identified by X-ray crystallography as previously reported $\{La[N(SiMe_3)_2]_4\}\{K(THF)_6\}$.[20] However, EPR studies of the orange filtrate gave an EPR spectrum consistent with $\{[(Me_3Si)_2N]_2La(THF)_x\}_2(\mu\text{-}\eta^2\text{:}\eta^2\text{-}N_2)[K(THF)_y]$, **7**, as described in the Results section. The ^{15}N analogue of **7**, that is, **7-^{15}N**, was prepared analogously from $^{15}N_2$ and gave the EPR spectrum expected for this change in isotope. THF solutions of **7** continue to exhibit the characteristic EPR pattern over the course of one month if they are stored at −35 °C. However, solutions decompose overnight at ambient temperature.

$\{[(Me_3Si)_2N]_2Y(THF)\}_2(\mu\text{-}\eta^2\text{:}\eta^2\text{-}N_2)[Na(THF)_6]$, 8. In a nitrogen-filled glovebox, a colorless solution of $Y[N(SiMe_3)_2]_3$ (220 mg, 0.38 mmol) in 10 mL of THF was syringed into a 100 mL round-bottom flask containing a 90:10 mixture of N_2 and H_2 gas (regeneration gas) by volume, an excess of sodium metal smeared on the bottom of the flask, and a stir bar. The reaction mixture immediately became orange. After the mixture was stirred for 3 h, it was centrifuged to remove insoluble material. Evaporation of the supernatant yielded an orange oil. At −35 °C over 2−3 d, a concentrated sample of the oil in 2 mL of diethyl ether produced yellow orange crystals of $\{[(Me_3Si)_2N]_2Y(THF)\}_2(\mu\text{-}\eta^2\text{:}\eta^2\text{-}N_2)[Na(THF)_6]$, **8**, and a small amount of blue crystals, presumably the $\{[(Me_3Si)_2N]_2(THF)Y\}_2(\mu\text{-}\eta^2\text{:}\eta^2\text{-}N_2)$ complex.[19,20]

$\{[(Me_3Si)_2N]_2Er(THF)\}_2(\mu\text{-}\eta^2\text{:}\eta^2\text{-}N_2)[Na(THF)_6]$, 9. In a nitrogen-filled glovebox, a pink solution of $Er[N(SiMe_3)_2]_3$ (1.14 g, 1.76 mmol) in 20 mL of THF was added dropwise to a flask containing a > 5-fold excess of sodium metal smeared on the bottom. The mixture immediately turned pale orange and after stirring for 3 h, the solution was yellow-brown. The mixture was centrifuged to remove any residual sodium metal, and evaporation of the supernatant yielded a dark pink solid. Crystals of **9** suitable for X-ray analysis were grown from a concentrated diethyl ether solution at −35 °C over the course of 3 d. This sample also contained pink crystals presumably of the previously characterized $\{[(Me_3Si)_2N]_2Er(THF)\}_2(\mu\text{-}\eta^2\text{:}\eta^2\text{-}N_2)$.[20]

Improved Synthesis of $\{[(Me_3Si)_2N]_2Y(THF)\}_2(\mu\text{-}\eta^2\text{:}\eta^2\text{-}N_2)$, 3. In a nitrogen-filled glovebox, KC_8 (1.04 g, 7.70 mmol) was added at ambient temperature to a vigorously stirred solution of $Y[N(SiMe_3)_2]_3$ (4.38 g, 7.68 mmol) in 100 mL of THF over the course of 3 min. The solution immediately became the orange color of $\{[(Me_3Si)_2N]_2Y(THF)\}_2(\mu\text{-}\eta^2\text{:}\eta^2\text{-}N_2)[K(THF)_6]$, **4a**, and the suspension was stirred for 10 min. The reaction mixture was centrifuged

(25) Bergbreiter, D. E.; Killough, J. M. *J. Am. Chem. Soc.* **1978**, *100*, 2126.
(26) Edelmann, F. T.; Poremba, P. In *Synthetic Methods of Organometallic and Inorganic Chemistry*; Herrmann, W. A., Ed.; Thieme Verlag: Stuttgart, Germany, 1997; Vol. *6*, p 37.
(27) Edelmann, F. T.; Poremba, P. In *Synthetic Methods of Organometallic and Inorganic Chemistry*; Herrmann, W. A., Ed.; Thieme Verlag: Stuttgart, Germany, 1997; Vol. *6*, p 41.
(28) Nilges, M. J.; Mattson, K. J.; Belford, R. L. In *ESR Spectroscopy in Membrane Biophysics, Biological Magnetic Resonance*; Hemminga, M. A., Berliner, L., Eds.; Springer: New York, 2006; Vol. *27*, p 261.

Table 1. X-ray Data Collection Parameters

	$C_{56}H_{136}KLu_2N_6O_8Si_8\cdot 2(C_4H_8O)$	$C_{56}H_{136}N_6NaO_8Si_8Y_2$	$C_{56}H_{136}N_6NaO_8Si_8Er_2$	$C_{52}H_{128}KN_6O_{10}Si_8Y_2\cdot 2(C_4H_8O)$	$C_{41}H_{93}KN_3O_7Si_6Y$
	6·2THF	**8**	**9**	**10**·2THF	**12**
formula weight	1779.68	1447.24	1603.94	1583.45	1036.73
T(K)	203(2)	163(2)	163(2)	148(2)	93(2)
crystal system	monoclinic	monoclinic	monoclinic	triclinic	monoclinic
space group	$P2_1/c$	$P2_1/c$	$P2_1/c$	$P\bar{1}$	$P2_1/c$
a (Å)	15.892(6)	12.860(3)	12.834(2)	10.4483(7)	12.0874(5)
b (Å)	24.148(9)	19.633(5)	19.587(3)	13.7447(9)	30.8857(12)
c (Å)	12.262(5)	16.079(4)	16.106(3)	16.9943(11)	15.7704(6)
α (deg)	90	90	90	70.4402(8)	90
β (deg)	91.982(5)	91.962(4)	92.120(2)	77.3142(8)	98.4181(5)
γ (deg)	90	90	90	70.8400(8)	90
volume Å^3	4703(3)	4057.5(16)	4046.1(11)	2155.7(2)	5824.1(4)
Z	2	2	2	1	4
ρ_{calcd} (Mg/m^3)	1.257	1.185	1.317	1.220	1.182
μ (mm^{-1})	2.279	1.592	2.229	1.550	1.238
R1 [$I > 2.0\sigma(I)$][a]	0.0445	0.0519	0.0225	0.0321	0.0293
wR2 (all data)[a]	0.1323	0.1514	0.0614	0.0828	0.0739

[a] Definitions: R1 = $\sum||F_o| - |F_c||/\sum|F_o|$, wR2 = $[\sum w(F_o^2 - F_c^2)^2/\sum w(F_o^2)^2]^{1/2}$.

and filtered to remove dark insoluble material, presumably graphite. Excess Hg (ca. 10 mL) was added to this orange filtrate and vigorously stirred for 3 h during which time the orange solution turned to the light blue color of $\{[(Me_3Si)_2N]_2Y(THF)\}_2(\mu\text{-}\eta^2\text{:}\eta^2\text{-}N_2)$, **3**. The solution was transferred to a 500 mL flask and concentrated to about 10 mL under vacuum. The concentrate appeared green (note yellow byproduct **11** in section below). After 1 d at −30 °C, $\{[(Me_3Si)_2N]_2Y(THF)\}_2(\mu\text{-}\eta^2\text{:}\eta^2\text{-}N_2)$, **3**, (0.653 g, 17%) was isolated as light blue crystals. The yellow green mother liquor was concentrated to about 5 mL and cooled to −30 °C for 1 d to yield a second crop of blue crystals of $\{[(Me_3Si)_2N]_2Y(THF)\}_2(\mu\text{-}\eta^2\text{:}\eta^2\text{-}N_2)$, **3**, (0.390 g, combined yield 27%).

To confirm the formation of potassium amalgam in the above reaction, Hg (433 mg, 2.16 mmol) was added to a stirred THF (10 mL) solution of $\{[(Me_3Si)_2N]_2Y(THF)\}_2(\mu_3\text{-}\eta^2\text{:}\eta^2\text{:}\eta^2\text{-}N_2)K$, **4b**, (255 mg, 0.247 mmol). After stirring overnight, the orange solution turned to pale blue green accompanied by solidification of the liquid mercury to a shiny metallic material (444 mg). The 11 mg weight increase is close to the calculated value, that is, 10 mg, for the amount of potassium that should be incorporated into Hg. NMR spectroscopy showed that $\{[(Me_3Si)_2N]_2Y(THF)\}_2(\mu\text{-}\eta^2\text{:}\eta^2\text{-}N_2)$, **3**, is the only other product of this reaction.

Synthesis of $\{[(Me_3Si)_2N]_2Y(THF)\}_2(\mu_3\text{-}\eta^2\text{:}\eta^2\text{:}\eta^2\text{-}N_2)K$, 4b, from $\{[(Me_3Si)_2N]_2Y(THF)\}_2(\mu\text{-}\eta^2\text{:}\eta^2\text{-}N_2)$, 3. THF (5 mL) was added to a 20 mL scintillation vial containing $\{[(Me_3Si)_2N]_2Y(THF)\}_2(\mu\text{-}\eta^2\text{:}\eta^2\text{-}N_2)$, **3**, (300 mg, 0.30 mmol), KC_8 (45 mg, 0.33 mmol), and a stir bar. After stirring for 5 min, the reaction mixture was centrifuged and filtered to remove dark insoluble material, presumably graphite. Removal of THF afforded $\{[(Me_3Si)_2N]_2Y(THF)\}_2(\mu_3\text{-}\eta^2\text{:}\eta^2\text{:}\eta^2\text{-}N_2)K$, **4b**, as a yellow orange powder (290 mg, 93%) identified by elemental analysis and EPR spectroscopy. When excess KC_8 (e.g., 3 equiv) was used, a colorless THF solution was obtained instead. The NMR spectrum of this reaction mixture showed 7 resonances in the 0.2−0.5 ppm region that did not correlate with known yttrium bis(trimethylsilyl) amide complexes.

$\{[(Me_3Si)_2N]_2Y(THF)\}_2(\mu\text{-}\eta^2\text{:}\eta^2\text{-}N_2)[K(18\text{-crown-}6)(THF)_2]$, 10. THF (10 mL) was added to a 20 mL scintillation vial containing $\{[(Me_3Si)_2N]_2Y(THF)\}_2(\mu\text{-}\eta^2\text{:}\eta^2\text{-}N_2)$, **3**, (310 mg, 0.312 mmol), KC_8 (43 mg, 0.32 mmol), 18-crown-6 (85 mg, 0.32 mmol), and a stir bar. After stirring for 5 min, the reaction mixture was centrifuged and filtered to remove a black material, presumably graphite. The orange filtrate was concentrated to about 2 mL, layered with 5 mL of hexane, and stored at −35 °C. $\{[(Me_3Si)_2N]_2Y(THF)\}_2(\mu\text{-}\eta^2\text{:}\eta^2\text{-}N_2)[K(18\text{-crown-}6)(THF)_2]$, **10**, (320 mg, 79%), was obtained as orange crystals after 1 d. IR: 2942s, 2892s, 1976w, 1707w, 1610w, 1472 m, 1454 m, 1352s, 1238s, 1183w, 1112s, 1014s, 967s, 872s, 828s, 769 m, 691w, 666s, 615s cm^{-1}. Anal. Calcd for $C_{44}H_{112}KN_6O_8Si_8Y_2$, **10**(−2THF): C, 40.81; H, 8.72; N, 6.49. Found: C, 40.61; H, 9.36; N, 6.04.

Metalated Byproducts in the Synthesis of 3: $\{[(Me_3Si)_2N]_2Y[CH_2Si(Me_2)NSiMe_3]\}[K(THF)_2]$, 11, and $\{[(Me_3Si)_2N]_2Y[CH_2Si(Me_2)NSiMe_3]\}[K(18\text{-crown-}6)(THF)(toluene)]$, 12. When THF was removed under vacuum from the mother liquor of the reaction described above in the section on an improved synthesis of **3**, a pale yellow oily material was isolated that was washed with cold hexanes (4 × 10 mL) to afford **11** (0.710 g, 0.964 mmol, 13%) as a yellow oil. 18-crown-6 (0.255 g, 0.964 mmol) was added to a toluene solution of **11** and the mixture was stored at −30 °C for 1 d. X-ray quality single crystals of $\{[(Me_3Si)_2N]_2Y[CH_2Si(Me_2)NSiMe_3]\}[K(18\text{-crown-}6)(THF)(toluene)]$, **12**, were obtained. For **11**: ^{1}H NMR (500 MHz, benzene-d_6): δ −1.16 (d, 2H, $^2J_{YH}$ = 2.2 Hz, C*H*$_2$SiMe$_2$NSiMe$_3$), 0.19 (s, 6H, CH$_2$Si*Me*$_2$NSiMe$_3$), 0.59 (s, 36H, N(Si*Me*$_3$)$_2$), 0.61 (s, 9H, CH$_2$SiMe$_2$NSi*Me*$_3$), 1.39 (bm, 8H, *THF*), 3.42 (bm, 8H, *THF*). ^{13}C NMR (126 MHz, benzene-d_6): δ 6.27 (s, N(Si*Me*$_3$)$_2$), 6.51 (s, CH$_2$SiMe$_2$NSi*Me*$_3$), 8.55 (d, $^3J_{YC}$ = 1.8 Hz, CH$_2$Si*Me*$_2$NSiMe$_3$), 24.1 (d, $^1J_{YC}$ = 24 Hz, *C*H$_2$SiMe$_2$NSiMe$_3$), 26.0 (s, *THF*), 68.2 (s, *THF*). For **12**: ^{1}H NMR (500 MHz, THF-d_8): δ −0.55 (d, 2H, $^2J_{YH}$ = 2.8 Hz, C*H*$_2$SiMe$_2$NSiMe$_3$), 0.01 (s, 15H, CH$_2$Si*Me*$_2$NSi*Me*$_3$), 0.12 (s, 36H, N(Si*Me*$_3$)$_2$), 3.62 (s, 24H, *18-crown-6*). ^{13}C NMR (126 MHz, THF-d_8): δ 6.03 (s, N(Si*Me*$_3$)$_2$), 6.34 (s, CH$_2$SiMe$_2$NSi*Me*$_3$), 7.85 (s, CH$_2$Si*Me*$_2$NSiMe$_3$), 27.1 (d, $^1J_{YC}$ = 33 Hz, *C*H$_2$SiMe$_2$NSiMe$_3$), 71.3 (*18-crown-6*). IR: 2946s, 2892s, 2827sh, 2797sh, 2746w, 2713w, 2691w, 1978w, 1840w, 1691w, 1605w, 1474 m, 1455 m, 1434 m, 1397w, 1353s, 1284sh, 1242s, 1113s, 1026s, 994s, 966s, 872s, 833s, 774s, 754s, 712s, 690s, 666s, 635w, 604s cm^{-1}. Anal. Calcd for $C_{30}H_{77}KN_3O_6Si_6Y$, **12**(−toluene,−THF): C, 41.30; H, 8.90; N, 4.82. Found: C, 41.40; H, 9.27; N, 4.58.

X-ray Crystallographic Data. Details are in Table 1 and the Supporting Information.

Computational Details. The computational strategy used in the present work extends the methods previously used to analyze $[(C_5Me_4H)_2Sc]_2(\mu\text{-}\eta^2\text{:}\eta^2\text{-}N_2)$,[24] $\{[(Me_3Si)_2N]_2Y(THF)\}_2(\mu\text{-}\eta^2\text{:}\eta^2\text{-}N_2)$, **3**,[1] and $\{[(Me_3Si)_2N]_2Y(THF)\}_2(\mu\text{-}\eta^2\text{:}\eta^2\text{-}N_2)[K(THF)_6]$, **4a**.[1]

The first attempt at a structural optimization of compounds **1** and **2a** was carried out with small core pseudopotentials[29] for the Dy atoms, but this proved difficult because of SCF convergence issues discussed below. Larger 4f-in-core pseudopotentials[30] and

(29) Andrae, D.; Haussermann, U.; Dolg, M. *Theor. Chim. Acta* **1990**, *77*, 123.
(30) Dolg, M.; Stoll, H.; Preuss, H. *Theor. Chim. Acta* **1993**, *85*, 441.

the quasi-relativistic basis sets of Dolg et al.[31] were then employed for Dy atoms in conjunction with split valence basis sets including polarization functions for non-hydrogen atoms (SV(P))[32] for the other atoms in the compound. The TPSSh[33] one-parameter hybrid meta-GGA functional was selected based on previous experience.[34,35] After that, the refined structures were computed using a larger triple-ζ valence basis with two sets of polarization functions on non-hydrogen atoms (def2-TZVP)[38] and tighter convergence thresholds, the results of which are the reported values for the calculated structural data. Differences in bond lengths between SV(P) and TZVP were less than 0.01 Å. Vibrational frequencies[39] were computed at the SV(P) level and scaled by 0.95 to account for anharmonicities.[1] All structures were confirmed to be minima by the absence of imaginary vibrational modes. Fine quadrature grids (size m4)[40] and C_i symmetry were used throughout. All computational results were obtained using the TURBOMOLE program package.[41] The structures of compounds $\{[(Me_3Si)_2N]_2Lu(THF)\}_2(\mu\text{-}\eta^2\text{:}\eta^2\text{-}N_2)$, **5**, and $\{[(Me_3Si)_2N]_2Lu(THF)\}_2(\mu\text{-}\eta^2\text{:}\eta^2\text{-}N_2)[K(THF)_6]$, **6**, were optimized with the same procedure, except that relativistic small-core pseudopotentials[29] (def-ecp) could be used for Lu because of the absence of open f shells. These small core pseudopotentials along with def-SV(P) and def-TZVP basis sets from the TURBOMOLE basis set library were used for the Lu atoms.

Results

$(N_2)^{2-}$ and $(N_2)^{3-}$ Complex Formation from $Dy(OAr)_3/KC_8/N_2$. Addition of $Dy(OAr)_3$ to KC_8 in THF under dinitrogen forms both the two-electron and three-electron reduced dinitrogen complexes, $[(ArO)_2Dy(THF)_2]_2(\mu\text{-}\eta^2\text{:}\eta^2\text{-}N_2)$, **1**, and $[(ArO)_2Dy(THF)]_2(\mu\text{-}\eta^2\text{:}\eta^2\text{-}N_2)[K(THF)_6]$, **2a**,[1] eq 1. Complex **1** was isolated by crystallization of the toluene extracts of the reaction mixture. Complex **2a** was isolated by crystallization from THF of the toluene insoluble part of the crude product. Both complexes were identified by X-ray crystallography since this is the most definitive method for these highly paramagnetic species. The products of eq 1

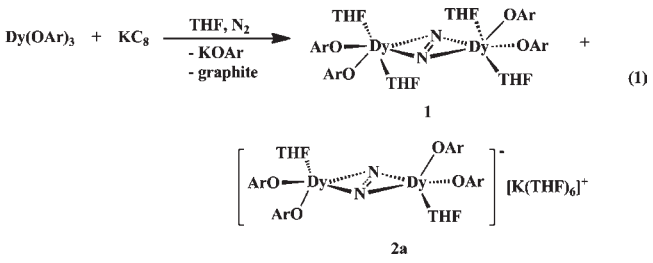

are the same species obtained from the $DyI_2/KOAr$ reaction shown in Scheme 1. The yield of **2a** in eq 1 is comparable to that obtained via Scheme 1, 29% versus 20%, while the yield of **1** is higher, 20% versus 3%. Since the yields are only reported on crystallographically characterizable material, they represent the capacity of the compounds to be crystallized rather than the yield in solution.

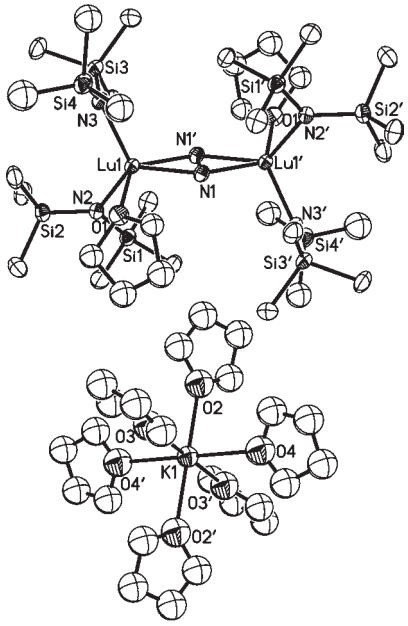

Figure 1. Thermal ellipsoid plot of $\{[(Me_3Si)_2N]_2Lu(THF)\}_2(\mu\text{-}\eta^2\text{:}\eta^2\text{-}N_2)[K(THF)_6]$, **6**, drawn at the 30% probability level. Hydrogen atoms are omitted for clarity.

$(N_2)^{3-}$ Formation from $Lu[N(SiMe_3)_2]_3/KC_8/N_2$ and $La[N(SiMe_3)_2]_3/KC_8/N_2$. Since it had previously been shown that variation of conditions of the $Y[N(SiMe_3)_2]_3/KC_8$ reaction could produce $(N_2)^{3-}$ as well as $(N_2)^{2-}$ products,[1] the $Ln[N(SiMe_3)_2]_3/KC_8$ reaction systems were re-examined with Ln = Lu and La in efforts to obtain more examples of $(N_2)^{3-}$ complexes with diamagnetic metal ions. The addition of $Lu[N(SiMe_3)_2]_3$ to KC_8 all at once under dinitrogen had previously been shown to make $\{[(Me_3Si)_2N]_2Lu(THF)\}_2(\mu\text{-}\eta^2\text{:}\eta^2\text{-}N_2)$, **5**, in 36% isolated yield by crystallization from diethyl ether. By adding KC_8 slowly over 20 min to $Lu[N(SiMe_3)_2]_3$, the yellow-orange $(N_2)^{3-}$ complex, $\{[(Me_3Si)_2N]_2Lu(THF)\}_2(\mu\text{-}\eta^2\text{:}\eta^2\text{-}N_2)[K(THF)_6]$, **6**, eq 2, Figure 1, could be isolated in 20% yield by crystallization from THF. The yellow orange color of the mother liquor indicated that additional amounts of **6** were still present and NMR spectroscopy confirmed the presence of **5** as well in the mother liquor.

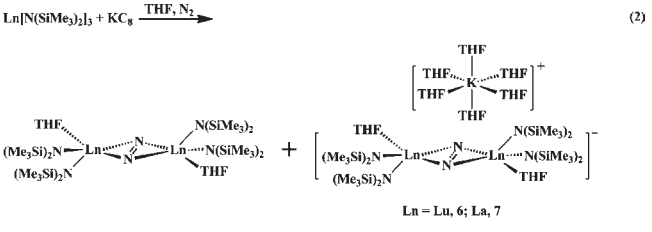

Analogous $(N_2)^{2-}$ and $(N_2)^{3-}$ products were obtained from the $La[N(SiMe_3)_2]_3/KC_8$ system, although in this case the reduced dinitrogen complexes were not obtained as crystalline solids. As previously reported, the main product isolated from this reaction is $\{La[N(SiMe_3)_2]_4\}\{K(THF)_6\}$,[20]

(31) Dolg, M.; Stoll, H.; Savin, A.; Preuss, H. *Theor. Chim. Acta* **1989**, *75*, 173.
(32) Schäfer, A.; Horn, H.; Ahlrichs, R. *J. Chem. Phys.* **1992**, *97*, 2571.
(33) Staroverov, V. N.; Scuseria, G. E.; Tao, J.; Perdew, J. P. *J. Chem. Phys.* **2003**, *119*, 12129.
(34) Evans, W. J.; Fang, M.; Bates, J. E.; Furche, F.; Ziller, J. W.; Kiesz, M. D.; Zink, J. I. *Nat. Chem.* **2010**, *2*, 644.
(35) TPSSh was chosen over B3LYP for the DFT calculations because the B3LYP functional contains 20% Hartree−Fock exchange and is not the method of choice for transition metal chemistry, particularly for systems with weakly occupied d orbitals. TPSSh, which includes 10% Hartree−Fock exchange, contains fewer fitted parameters, satisfies more exact constraints, and statistically outperforms B3LYP for energetics and structures of transition metal complexes.[36,37]
(36) Furche, F.; Perdew, J. P. *J. Chem. Phys.* **2006**, *124*, 044103(1).
(37) Bühl, M.; Kabrede, H. *J. Chem. Theory Comput.* **2006**, *2*, 1282.
(38) Weigend, F.; Ahlrichs, R. *Phys. Chem. Chem. Phys.* **2005**, *18*, 3297.
(39) Deglmann, P.; Furche, F.; Ahlrichs, R. *Chem. Phys. Lett.* **2002**, *362*, 511.
(40) Treutler, O.; Ahlrichs, R. *J. Chem. Phys.* **1995**, *102*, 346.
(41) *TURBOMOLE*, V6−2; TURBOMOLE GmbH: Karlsruhe, Germany, 2010; http://www.turbomole.com

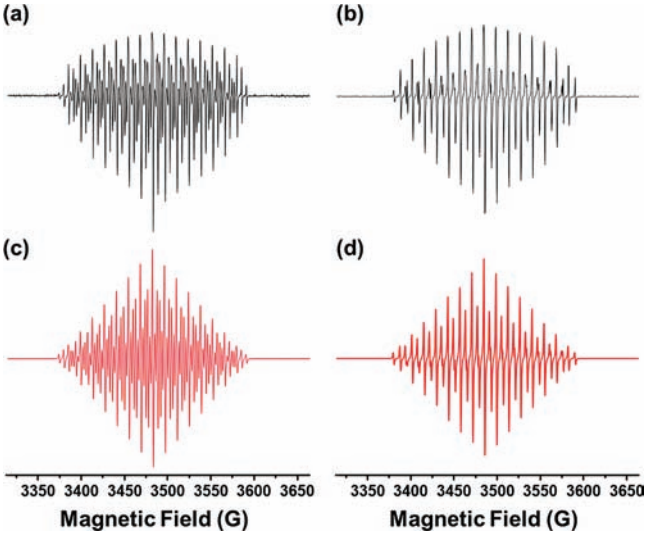

Figure 2. EPR spectra of $\{[(Me_3Si)_2N]_2La(THF)_x\}_2(\mu\text{-}\eta^2\text{:}\eta^2\text{-}N_2)[K(THF)_y]$, **7**: (a) **7** at 293 K in millimolar THF solution, (b) **7-^{15}N** at 293 K in millimolar THF solution, (c) simulation of (a), and (d) simulation of (b).

the product that forms when the $KN(SiMe_3)_2$ byproduct of a $Ln[N(SiMe_3)_2]_3/KC_8$ reduction combines with the $Ln[N(SiMe_3)_2]_3$ starting material. The formation of $\{La[N(SiMe_3)_2]_4\}\{K(THF)_6\}$ may be facilitated by the large size of lanthanum compared to the lanthanides later in the series. Evidence for dinitrogen reduction in this reaction was originally obtained via ^{15}N NMR spectroscopy which indicated the formation of the $\{[(Me_3Si)_2N]_2La(THF)_x\}_2(\mu\text{-}\eta^2\text{:}\eta^2\text{-}N_2)$ analogue of compounds previously characterized by X-ray crystallography for Nd, Gd, Tb, Dy, Y, Ho, Er, Tm, and Lu.[20]

In this study, the slow addition method of adding KC_8 to $La[N(SiMe_3)_2]_3$ was used and evidence for an $(N_2)^{3-}$ product, $\{[(Me_3Si)_2N]_2La(THF)_x\}_2(\mu\text{-}\eta^2\text{:}\eta^2\text{-}N_2)[K(THF)_y]$, **7**, was obtainable by EPR spectroscopy, Figure 2a. The spectrum contains a signal at $g = 2.0025$ that has a multiline pattern due to splitting by two ^{14}N ($I = 1$) and two ^{139}La ($I = 7/2$) nuclei. To simplify the spectrum and aid in simulation studies, an analogous reaction was conducted with $^{15}N_2$, and its spectrum is shown in Figure 2b. Simulations of **7** and **7-^{15}N** (Figures 2c and 2d, respectively) provide the hyperfine coupling constants of 5.5 G for ^{14}N, 7.7 G for ^{15}N, and 13.9 G for ^{139}La. These nitrogen coupling constants are similar to the 5.8−8.2 G values found in the analogous yttrium complexes.[1] The 13.9 G lanthanum coupling constant is much smaller than the 133.5 G value reported for a La^{2+} compound,[42] which is consistent with a dinitrogen centered radical bridging two diamagnetic La^{3+} ions in **7**.

$(N_2)^{3-}$ Formation from $Ln[N(SiMe_3)_2]_3/Na/N_2$. The $(N_2)^{3-}$ complexes **2a** and **2b** in Scheme 1 were isolated as potassium salts since the $DyI_2/2KOAr$ reaction involved a potassium salt precursor. The yttrium $(N_2)^{3-}$ complexes, **4a** and **4b**, in Scheme 2 and the lutetium complex, **6**, in eq 2 were also isolated as potassium salts since the reducing metal, M, in these LnA_3/M reactions was potassium. In the past, it had been shown that LnA_3/M methods could make $(N_2)^{2-}$ complexes with M = Na,[20] and it was of interest to determine if sodium reactions could also make $(N_2)^{3-}$ complexes.

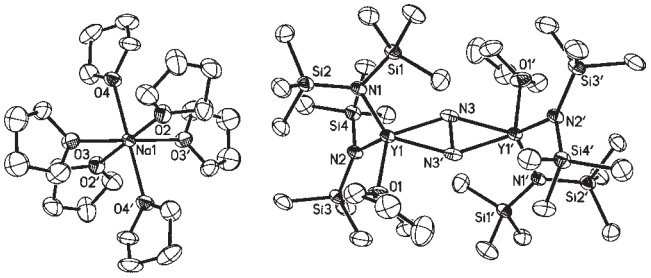

Figure 3. Thermal ellipsoid plot of $\{[(Me_3Si)_2N]_2Y(THF)\}_2(\mu\text{-}\eta^2\text{:}\eta^2\text{-}N_2)[Na(THF)_6]$, **8**, drawn at the 50% probability level. Hydrogen atoms are omitted for clarity. The structure of the erbium analogue, **9**, is isomorphous.

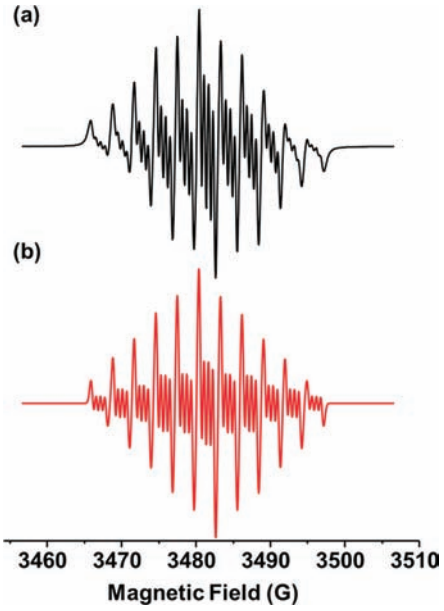

Figure 4. EPR spectrum of $\{[(Me_3Si)_2N]_2Y(THF)\}_2(\mu\text{-}\eta^2\text{:}\eta^2\text{-}N_2)[Na(THF)_6]$, **8**: (a) **8** at 293 K in millimolar toluene solution, (b) the simulated spectrum.

Crystalline samples of yellow orange $\{[(Me_3Si)_2N]_2Y(THF)\}_2(\mu\text{-}\eta^2\text{:}\eta^2\text{-}N_2)[Na(THF)_6]$, **8**, and orange $\{[(Me_3Si)_2N]_2Er(THF)\}_2(\mu\text{-}\eta^2\text{:}\eta^2\text{-}N_2)[Na(THF)_6]$, **9**, were isolated as byproducts along with the corresponding pale blue yttrium[20] and pink erbium[20] $(N_2)^{2-}$ complexes, $\{[(Me_3Si)_2N]_2Ln(THF)\}_2(\mu\text{-}\eta^2\text{:}\eta^2\text{-}N_2)$, from reactions of $Ln[N(SiMe_3)_2]_3$ with sodium in THF under N_2 atmosphere at room temperature. Complexes **8** and **9** were characterized by X-ray crystallography and found to be isomorphous, Figure 3. The EPR spectrum of **8** was obtained in toluene as shown in Figure 4. An 11-line pattern is observed that can be explained by simulation to arise from splitting by two ^{89}Y ($I = 1/2$) and two ^{14}N ($I = 1$) nuclei as well as quartet features due to interaction of the unpaired electron with an $I = 3/2$ ^{23}Na nucleus. The coupling to sodium suggests that the Na^+ ion loses THF in toluene solution and interacts with the $(N_2)^{3-}$ ligand as observed crystallographically in the potassium analogue, $\{[(Me_3Si)_2N]_2Y(THF)\}_2(\mu_3\text{-}\eta^2\text{:}\eta^2\text{:}\eta^2\text{-}N_2)K$, **4b**, Scheme 2.[1] Simulation of the EPR spectrum of **8** in toluene provides the hyperfine coupling constants of 0.60 G for ^{23}Na, 2.9 G for ^{89}Y, and 5.8 G for ^{14}N. The ^{89}Y and ^{14}N coupling constants match the 3.1 and 5.8 G values obtained with $\{[(Me_3Si)_2N]_2Y(THF)\}_2(\mu_3\text{-}\eta^2\text{:}\eta^2\text{:}\eta^2\text{-}N_2)K$, **4b**, and

(42) Hitchcock, P. B.; Lappert, M. F.; Maron, L.; Protchenko, A. V. *Angew. Chem., Int. Ed.* **2008**, *47*, 1488.

the ^{23}Na coupling constant is close to the 1.05 G value reported for $Na[(CH_3)_3SiN=NSi(CH_3)_3]$.[43] The 5.8 G coupling constant for ^{14}N in **8** is also similar to the 4.0 G value calculated by DFT.

Improved Synthesis of $\{[(Me_3Si)_2N]_2Y(THF)\}_2(\mu$-$\eta^2$:$\eta^2$-$N_2)$, 3. Since the $(N_2)^{3-}$ products like **2a**, **2b**, **4a**, and **4b**, which we will generically abbreviate as Ln_2N_2M, are further reduced versions of the $(N_2)^{2-}$ products like **1** and **3**, which we will designate as Ln_2N_2, it was conceivable that mild oxidation of the Ln_2N_2M/Ln_2N_2 mixtures could convert Ln_2N_2M to Ln_2N_2. Indeed, $\{[(Me_3Si)_2N]_2Y(THF)\}_2(\mu$-$\eta^2$:$\eta^2$-$N_2)[K(THF)_6]$, **4a**, can be cleanly converted back to $\{[(Me_3Si)_2N]_2Y(THF)\}_2(\mu$-$\eta^2$:$\eta^2$-$N_2)$, **3**, in the presence of mercury eq 3. This reaction also forms a metallic solid product with the weight and

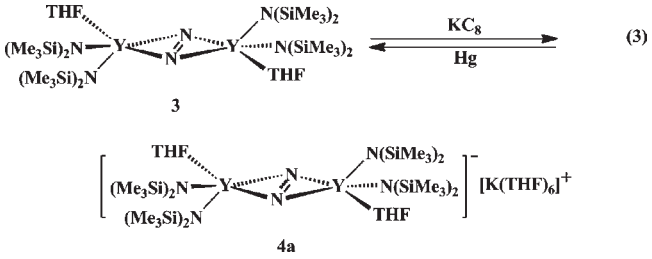

consistency expected for potassium amalgam that is easily separated by decantation. This reaction can be utilized to increase the yield of Y_2N_2 if the $(N_2)^{2-}$ complex is the desired reaction product. For example, $\{[(Me_3Si)_2N]_2Y(THF)\}_2(\mu$-$\eta^2$:$\eta^2$-$N_2)$, **3**, can be obtained in 27% overall yield, versus 18% as reported previously,[19] with the proper sequence (see below) of KC_8 addition and subsequent Hg oxidation. The fact that potassium amalgam does not react with **3** to make **4a** is consistent with these results.

Improved Synthesis of $\{[(Me_3Si)_2N]_2Y(THF)\}_2(\mu_3$-$\eta^2$:$\eta^2$:$\eta^2$-$N_2)$K, 4b. Since the Ln_2N_2M complexes are further reduced versions of the Ln_2N_2 complexes, it was conceivable that further reduction could increase the yield of Ln_2N_2M. Indeed, direct reduction of isolated $\{[(Me_3Si)_2N]_2Y(THF)\}_2$-$(\mu$-$\eta^2$:$\eta^2$-$N_2)$, **3**, by KC_8 in THF formed **4a**, eq 3. Removal of THF gave **4b** in 93% yield.

Since the LnA_3/M reactions inherently involve conditions under which initially formed Ln_2N_2 could be further reduced to Ln_2N_2M, methods to improve the yield of Ln_2N_2M directly that avoided the isolation of Ln_2N_2 and its subsequent reduction were investigated. In the $Y[N(SiMe_3)_2]_3/KC_8$ system, variations in the sequence of the reaction, the amount of KC_8 added, and the rate of addition of KC_8 were all examined. From these studies, it was found that the rate of addition of KC_8 to $Y[N(SiMe_3)_2]_3$ was the major factor that affected the yield of **3** versus **4a**. Slow addition of KC_8 to $Y[N(SiMe_3)_2]_3$ significantly increases the yield of **4a**. Normally, it would be expected that the reverse order, namely, addition of $Y[N(SiMe_3)_2]_3$ to KC_8, would enhance the formation of **4a**, since initially formed **3** could be directly reduced to **4a** by the local excess of KC_8. However, excess KC_8 decomposes **4a** to new products observable, but not identifiable, by NMR spectroscopy. Hence, the success of the slow addition method can be rationalized in a scenario in which **3** is gradually formed and additional KC_8 can reduce **3**

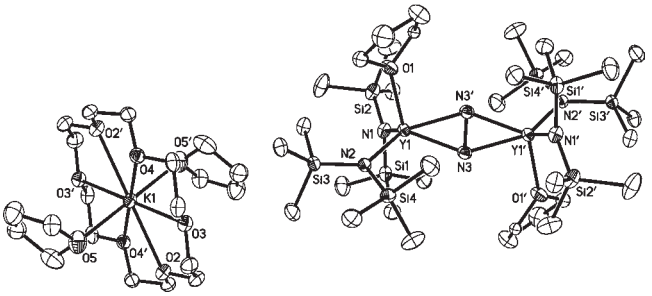

Figure 5. Thermal ellipsoid plot of $\{[(Me_3Si)_2N]_2Y(THF)\}_2(\mu$-$\eta^2$:$\eta^2$-$N_2)[K(18\text{-crown-}6)(THF)_2]$, **10**, drawn at the 50% probability level. Hydrogen atoms are omitted for clarity.

to **4a** or reduce more $Y[N(SiMe_3)_2]_3$ to make **3**. This avoids contact of **4a** with excess KC_8.

$\{[(Me_3Si)_2N]_2Y(THF)\}_2(\mu$-$\eta^2$:$\eta^2$-$N_2)[K(18$-crown-6)-$(THF)_2]$, 10. Manipulation of the $(N_2)^{2-}/(N_2)^{3-}$ mixture via solubility was also examined. Since it has been shown that crown ethers can help to stabilize and crystallize reactive complexes in which an alkali metal cation is the counterion,[42] reactions in the presence of crown ether were examined. The crown ether adduct, $\{[(Me_3Si)_2N]_2Y(THF)\}_2(\mu$-$\eta^2$:$\eta^2$-$N_2)$-$[K(18\text{-crown-}6)(THF)_2]$, **10**, was synthesized from the reaction of $\{[(Me_3Si)_2N]_2Y(THF)\}_2(\mu$-$\eta^2$:$\eta^2$-$N_2)$, **3**, with KC_8 in the presence of 18-crown-6, eq 4, and characterized by X-ray crystallography, Figure 5. It was found that **10** is much less soluble in THF than its parent compound, $\{[(Me_3Si)_2N]_2$-$Y(THF)\}_2(\mu$-η^2:η^2-$N_2)[K(THF)_6]$, **4a**. As a result, complex **10** can be more conveniently purified by recrystallization in a THF/hexane mixture at low temperature. In this case, **10** is initially precipitated and the small amount of residual **3** remains in solution.

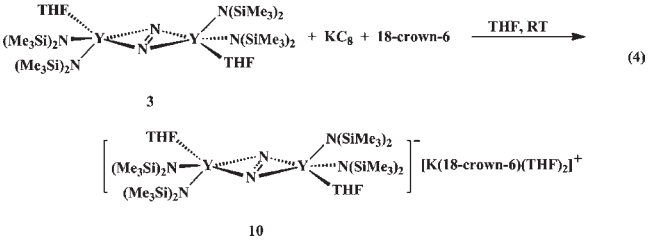

Isolation of a Ligand Degradation Byproduct, $\{[(Me_3Si)_2$-$N]_2Y[CH_2Si(Me_2)NSiMe_3]\}[K(THF)_2]$, 11. In the course of these studies, yet another product was found in the $Y[N$-$(SiMe_3)_2]_3/KC_8/N_2$ reaction mixture. NMR evidence was found for a cyclometalated byproduct, $\{[(Me_3Si)_2N]_2Y$-$[CH_2Si(Me_2)NSiMe_3]\}[K(THF)_2]$, **11**, that contains a previously reported anion, $\{[(Me_3Si)_2N]_2Y[CH_2Si(Me_2)$-$NSiMe_3]\}^-$ isolated from the reaction of $Y[N(SiMe_3)_2]_3$ with $KSi(SiMe_3)_3$ as a $[K(C_6H_6)_2]^{1+}$ salt.[44] Since **11** could only be isolated as an oil from THF, 18-crown-6 was added to enhance crystallinity. Single crystals of the 18-crown-6 adduct, $\{[(Me_3Si)_2N]_2Y[CH_2Si(Me_2)NSiMe_3]\}[K(18$-crown-6)(THF)(toluene)], **12**, were obtained and the presence of a metalated amide ligand, $[CH_2Si(Me_2)NSiMe_3]^{2-}$,[45−48]

(43) Krynitz, U.; Gerson, F.; Wiberg, N.; Veith, M. *Angew. Chem., Int. Ed. Engl.* **1969**, *8*, 755.

(44) Niemeyer, M. *Inorg. Chem.* **2006**, *45*, 9085.

(45) Karl, M.; Harms, K.; Seybert, G.; Massa, W.; Fau, S.; Frenking, G.; Dehnicke, K. *Z. Anorg. Allg. Chem.* **1999**, *625*, 2055.

(46) Deacon, G. B.; Forsyth, C. M. *Chem. Commun.* **2002**, 2522.

(47) Wang, J.; Gardiner, M. G. *Chem. Commun.* **2005**, 1589.

(48) Deacon, G. B.; Forsyth, C. M.; Junk, P. C.; Wang, J. *Inorg. Chem.* **2007**, *46*, 10022.

was confirmed by X-ray crystallography, Figure 6. Compound **12** had similar metrical parameters to those of $\{[(Me_3Si)_2N]_2Y[CH_2Si(Me_2)NSiMe_3]\}[K(C_6H_6)_2]$.[44] The η^2 binding mode of the toluene in [K(18-crown-6)(THF)-(toluene)]$^{1+}$ in **12** is similar to that found in other toluene adducts of potassium encircled by a crown ether as in $\{[Ce(\eta^5\text{-}C_5H_4SiMe_2{}^tBu)_3]_2(\mu\text{-}H)\}[K(18\text{-crown-6})(toluene)_2]$[49] and $\{Ca[N(SiMe_3)_2]_3\}[K(18\text{-crown-6})(THF)(toluene)]$,[50] but it differs from the η^1 bonding mode of toluene in $[Er(\eta^2\text{-}3,5\text{-di-}tert\text{-butyl pyrazolate})_4][K(18\text{-crown-6})\text{-}(DME)(toluene)]$.[51] This suggests that the presence of monodentate THF or bidentate toluene versus bidentate DME on one side of the crown ether can influence toluene coordination on the other side.

Structural Parameters of the $(N_2)^{3-}$ Complexes. Table 2 presents a comparison of the structures of the new $(N_2)^{3-}$ complexes **6**, **8**, **9**, and **10** with those of the previously reported **2a**, **2b**, **4a**, and **4b**.[1] The 1.393(7)−1.414(8) Å range of N−N distances listed in Table 2 is very narrow and matches also the distances of 1.396(7)−1.405(3) in previously isolated $(N_2)^{3-}$ complexes.[1] These distances are all longer than the 1.233-(5)−1.305(6) Å[7,13,19−23,52−54] range for $(N_2)^{2-}$ complexes, as is appropriate for a more reduced system.

The distances between the $(N_2)^{3-}$ ligand and Y, Er, and Lu are also similar when the differences in ionic radii are considered: Y^{3+} (0.900 Å), Er^{3+} (0.890 Å), and Lu^{3+} (0.861 Å; all values for 6 coordinate ions).[55] The

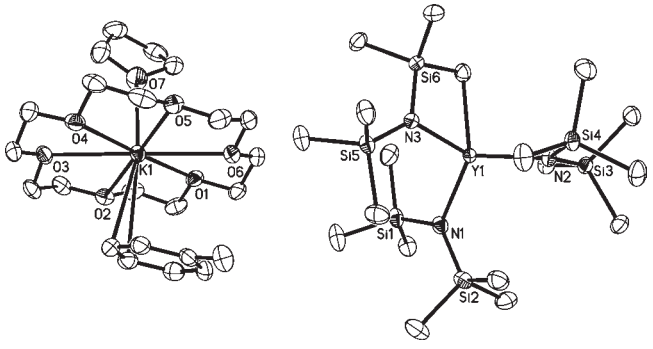

Figure 6. Thermal ellipsoid plot of $\{[(Me_3Si)_2N]_2Y[CH_2Si(Me_2)\text{-}NSiMe_3]\}[K(18\text{-crown-6})(THF)(toluene)]$, **12**, drawn at the 50% probability level. Hydrogen atoms are omitted for clarity.

2.197(3)−2.235(5) Å Dy−N distances in **2a** and **2b** are very similar to the Y−N analogues in **4a** and **4b**. Since the 6 coordinate ionic radius of Dy^{3+}, 0.912 Å, is very close to that of Y^{3+}, this indicates that there is little perturbation of the Ln_2N_2 core as the ancillary ligands are varied from aryloxide to amide.

DFT Analysis. The synthesis and isolation of $\{[(Me_3Si)_2\text{-}N]_2Lu(THF)\}_2(\mu\text{-}\eta^2\text{:}\eta^2\text{-}N_2)[K(THF)_6]$, **6**, provided a good opportunity to examine the bonding in a lanthanide dinitrogen species since Lu^{3+} is a closed shell ion. Previously, DFT analysis had been done only on $(N_2)^{2-}$ complexes of $3d^0$ Sc^{3+}[24] and $(N_2)^{2-}$ and $(N_2)^{3-}$ complexes of $4d^0$ Y^{3+}.[1] The $4f^{14}$ Lu^{3+} system, which has a high-lying 5d orbital, would allow a comparison of d orbital effects as a function of principal quantum number. The electronic structures of these reduced dinitrogen lanthanide complexes were evaluated with Kohn−Sham density functional theory using the TPSSh[33,35] functional as previously described.[1]

The structure of **6** was optimized without counterions. The computed N−N distance of 1.404 Å differs from the experimental value by less than 0.02 Å, while the average Lu−N distance differs by less than 0.03 Å, Table 3. Inspection of the Kohn−Sham orbitals for **6** shows a bonding interaction between the 5d orbitals of the metal and the π^* orbitals of the bridging N_2 ligand. As in the yttrium analogue, $\{[(Me_3Si)_2N]_2Y(THF)\}_2(\mu\text{-}\eta^2\text{:}\eta^2\text{-}N_2)$, **3**,[1] this interaction is possible because of (a) a good energy match between the N_2 π^* orbitals and the high energy Lu 5d orbitals, (b) the large size of the 5d orbitals, and (c) their symmetry appropriate for the nodal structure of the N_2 π^* orbitals, Figure 7a. The singly occupied molecular orbital (SOMO) of **6** is the formerly unperturbed π^* lowest unoccupied molecular orbital (LUMO) in $\{[(Me_3Si)_2N]_2Lu(THF)\}_2(\mu\text{-}\eta^2\text{:}\eta^2\text{-}N_2)$, **5**, which fits within the previously postulated[1] frontier molecular orbital (MO) scheme for **3** and **4a**. Further support for this MO scheme is seen in the computed spin density of **6**, which is confined to this SOMO, Figure 7b. Natural population analysis (NPA)[56] gives the Lu 5d/4f populations as 0.906/13.993 for **5** and 0.919/13.992 for **6** suggesting a full 4f shell and $5d^1$ occupation in both complexes. This is analogous to the yttrium compounds, **3** and **4a**, whose NPA suggests a $4d^1$ configuration.

Table 2. Selected Bond Lengths (Å) and Angles (deg) in **2a**, **2b**, **4a**, **4b**, **6**, **8**, **9**, and **10**

compounds	N−N	Ln−N	Ln−O/Ln−N	Ln−O (THF)	N−Ln−N′	Ln−N−Ln′
$[(ArO)_2Dy(THF)]_2$ ($\mu\text{-}\eta^2\text{:}\eta^2\text{-}N_2$)$[K(THF)_6]$, **2a**	1.396(7)	2.197(3)	2.154(2)	2.434(3)	37.0(2)	143.0(2)
		2.203(4)	2.158(2)			
$[(ArO)_2Dy(THF)]_2$ ($\mu_3\text{-}\eta^2\text{:}\eta^2\text{:}\eta^2\text{-}N_2$)K(THF), **2b**	1.402(7)	2.209(5)	2.148(4)	2.390(4)	36.7(2)	142.2(2)
		2.220(5)	2.151(4)	2.398(4)	36.8(2)	143.2(2)
		2.234(5)	2.160(4)			
		2.235(5)	2.168(4)			
$\{[(Me_3Si)_2N]_2Y(THF)\}_2$ ($\mu\text{-}\eta^2\text{:}\eta^2\text{-}N_2$)$[K(THF)_6]$, **4a**	1.401(6)	2.194(3)	2.303(3)	2.425(3)	37.0(2)	143.0(2)
		2.218(3)	2.341(3)			
$\{[(Me_3Si)_2N]_2Y(THF)\}_2$ ($\mu_3\text{-}\eta^2\text{:}\eta^2\text{:}\eta^2\text{-}N_2$)K, **4b**	1.405(3)	2.225(2)	2.328(2)	2.384(2)	36.57(8)	140.8(1)
		2.231(2)	2.329(2)	2.419(2)	36.67(9)	140.8(1)
		2.242(2)	2.331(2)			
		2.247(2)	2.341(2)			
$\{[(Me_3Si)_2N]_2Lu(THF)\}_2$ ($\mu\text{-}\eta^2\text{:}\eta^2\text{-}N_2$)$[K(THF)_6]$, **6**	1.414(8)	2.163(4)	2.265(4)	2.351(4)	38.0(2)	142.0(2)
		2.180(4)	2.285(4)			
$\{[(Me_3Si)_2N]_2Y(THF)\}_2$ ($\mu\text{-}\eta^2\text{:}\eta^2\text{-}N_2$)$[Na(THF)_6]$, **8**	1.393(7)	2.199(4)	2.328(4)	2.426(3)	36.8(2)	143.2(2)
		2.213(4)	2.334(4)			
$\{[(Me_3Si)_2N]_2Er(THF)\}_2$ ($\mu\text{-}\eta^2\text{:}\eta^2\text{-}N_2$)$[Na(THF)_6]$, **9**	1.403(4)	2.182(2)	2.303(2)	2.411(2)	37.34(9)	142.66(9)
		2.202(2)	2.318(2)			
$\{[(Me_3Si)_2N]_2Y(THF)\}_2$ ($\mu\text{-}\eta^2\text{:}\eta^2\text{-}N_2$) $[K(18\text{-crown-6})(THF)_2]$, **10**	1.396(3)	2.191(2)	2.315(2)	2.430(1)	36.95(8)	143.06(8)
		2.214(2)	2.343(2)			

Table 3. Experimental and Computed TPSSh/TZVP Bond Distances and Computed TPSSh/SV(P) Vibrational Frequencies (Scaled)[a]

compound	d(N−N) (Å) exp	d(N−N) (Å) calc	d(Ln−N) (Å) exp	d(Ln−N) (Å) calc	ν(N−N) (cm^{-1})
$[(ArO)_2Dy(THF)_2]_2$ (μ-η^2:η^2-N_2), **1**	1.257(7)	1.250	2.328(4)	2.398	1526
			2.340(4)	2.400	
$[(ArO)_2Dy(THF)]_2$ (μ-η^2:η^2-N_2)[$K(THF)_6$], **2a**	1.396(7)	1.392	2.197(3)	2.232	962
			2.203(4)	2.255	
$\{[(Me_3Si)_2N]_2Lu(THF)\}_2$ (μ-η^2:η^2-N_2), **5**	1.285(4)	1.256	2.241(2)	2.272	1451
			2.272(2)	2.294	
$\{[(Me_3Si)_2N]_2Lu(THF)\}_2$ (μ-η^2:η^2-N_2)[$K(THF)_6$], **6**	1.414(8)	1.404	2.163(4)	2.160	979
			2.180(4)	2.186	

[a] Energy converged to 10^{-7} a.u., density matrix converged to 10^{-6}.

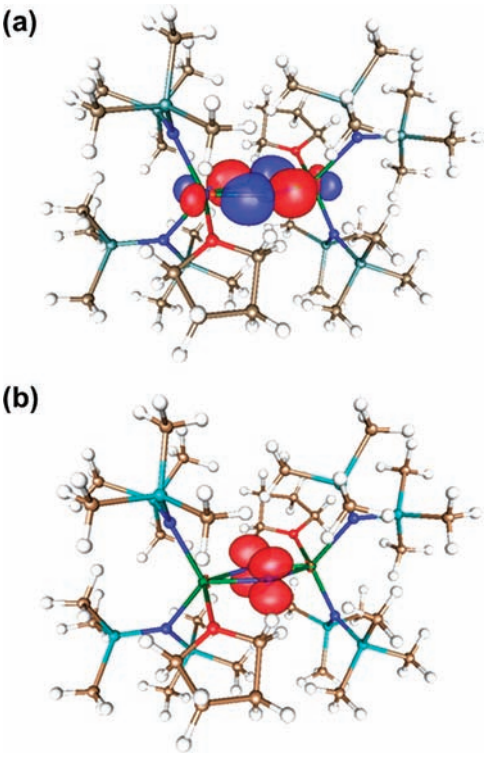

Figure 7. (a) SOMO-1 of $\{[(Me_3Si)_2N]_2Lu(THF)\}_2(\mu$-$\eta^2$:$\eta^2$-$N_2)$[K-$(THF)_6$], **6**, showing the 5d to π^* interaction. The contour value is 0.05. (b) Spin density of **6** computed at the def2-SV(P) level. Most of the spin density is confined to the unperturbed antibonding π^* orbital (SOMO) perpendicular to the Lu_2N_2 plane. The contour value is 0.005.

The more challenging open shell $[(ArO)_2Dy(THF)_2]_2$-(μ-η^2:η^2-N_2), **1**, and $[(ArO)_2Dy(THF)]_2$(μ-η^2:η^2-N_2)[K-$(THF)_6$], **2a**, have also been evaluated with DFT calculations. Larger 4f-in-core pseudopotentials, which include the 4f shell, were used for compounds **1** and **2a**, corresponding to a fixed $4f^9$ configuration of the Dy ions. This 4f occupation was chosen based upon the NPA results of converged single-point energy calculations of both compounds using small-core pseudopotentials for Dy. These 4f-in-core pseudopotentials were also tested on the Lu compounds, which are not affected by open f shells. The computed bond lengths for the dinitrogen bridge in **1** and **2a** differ by less than 0.01 Å from the experimental values while the Dy−N distances are roughly 0.06 Å too long for both oxidation states, Table 3. NPA for **1** and **2a** yields a 5d occupation of 0.770 and 0.729, respectively, in line with the chemical trend for Lu and Y. The MO and spin density plots for **2a** are very similar to those in Figure 7 and are only given in the Supporting Information. Hence, the 5d orbitals in open shell Dy^{3+} are also the primary source of bonding to dinitrogen.

Currently implemented SCF techniques[57] are slowly convergent for open f shells therefore limiting the success of working with full valence Dy metal centers. For the earliest attempts on **1** and **2a**, each calculation required in excess of 700 cycles with constant monitoring and manual shifting of the virtual orbitals. Using larger pseudopotentials avoids this problem and greatly reduced the number of SCF cycles necessary for convergence. These 4f-in-core pseudopotentials were also tested on **5** and **6**. Bond lengths computed with the larger pseudopotentials differ by less than 0.05 Å compared to the results obtained with small-core pseudopotentials. Thus, as pointed out by Dolg and co-workers[31,58] the use of 4f-in-core pseudopotentials is a pragmatic solution to SCF convergence problems in rare earth compounds with a fixed f electron configuration.

Discussion

The formation of $[(ArO)_2Dy(THF)_2]_2$(μ-η^2:η^2-N_2), **1**, and $[(ArO)_2Dy(THF)]_2$(μ-η^2:η^2-N_2)[$K(THF)_6$], **2a**, by the reduction of dinitrogen with the $Dy(ArO)_3/KC_8$ combination shows that the LnA_3/M method can be successfully carried out with aryloxide ligands as well as with amide and cyclopentadienyl ligands. However, the generality of the $Ln(OAr)_3/M$ reaction remains unknown since crystalline reduced dinitrogen complexes were not isolated with Ln = Y, La, and Lu. As seen previously with $Ln[N(SiMe_3)_2]_3/KC_8$ reactions,[20] the fact that a crystalline product could not be isolated and structurally characterized does not mean the reaction does not occur. However, with complexes of this type we prefer to use crystallographic evidence as the standard that establishes the viability of the synthesis.

One possible explanation for the difference in $Ln(OAr)_3/KC_8$ reactivity with Ln = Dy versus Y, La, and Lu, is that with

(49) Gun'ko, Y. K.; Hitchcock, P. B.; Lappert, M. F. *Organometallics* **2000**, *19*, 2832.
(50) He, X.; Allan, J. F.; Noll, B. C.; Kennedy, A. R.; Henderson, K. W. *J. Am. Chem. Soc.* **2005**, *127*, 6920.
(51) Deacon, G. B.; Delbridge, E. E.; Forsyth, C. M. *Angew. Chem., Int. Ed.* **1999**, *38*, 1766.
(52) Evans, W. J.; Zucchi, G.; Ziller, J. W. *J. Am. Chem. Soc.* **2003**, *125*, 10.
(53) Evans, W. J.; Allen, N. T.; Ziller, J. W. *Angew. Chem., Int. Ed.* **2002**, *41*, 359.
(54) Evans, W. J.; Allen, N. T.; Ziller, J. W. *J. Am. Chem. Soc.* **2001**, *123*, 7927.
(55) Shannon, R. D. *Acta Crystallogr.* **1976**, *A32*, 751.
(56) Reed, A. E.; Weinstock, R. B.; Weinhold, F. *J. Chem. Phys.* **1985**, *83*, 735.
(57) Csaszar, P.; Pulay, P. *J. Mol. Struct.* **1984**, *114*, 31.
(58) Dolg, M.; Stoll, H.; Prebys, E. *J. Mol. Struct.* **1991**, *235*, 67.

aryloxide ligands, the success of the reaction depends on the accessibility through a Ln^{2+} intermediate. Molecular Dy^{2+} complexes[59] are more accessible than La^{2+} complexes[42,60] and molecular Y^{2+} and Lu^{2+} complexes have not been reported in the literature. It is possible that when the metal is more difficult to reduce, the alkali metal reduces the aryloxide ligand and the reaction takes a different course. Since LnA_3/M reactions are successful with Y, La, and Lu with A = amide and cyclopentadienide, this argument must be specific to aryloxides. Arnold and co-workers have shown that the analogous $LnA_2A'/KC_8/N_2$ reaction was unsuccessful with A = $N(SiMe_3)_2$, A′ = ^{t}BuNCH$_2$−CH$_2${C(NCHCHN^{t}Bu)}, and Ln = Y.[61] It is quite reasonable that the success of the LnA_3/M method must depend on the stability of A to reduction. For example, Gambarotta and co-workers have shown attempts to reduce metals with strong reducing reagents such as lithium naphthalenide or NaH can instead result in reduction of an aromatic ligand.[62]

The isolation of $\{[(Me_3Si)_2N]_2Lu(THF)\}_2(\mu\text{-}\eta^2\text{:}\eta^2\text{-}N_2)[K(THF)_6]$, **6**, shows that the methods used in Scheme 2 are not limited to yttrium. Although yttrium is very similar to the late lanthanides and often used interchangeably, it is important to remember that it really is a transition metal with 4d orbitals at different energies than the high lying 5d orbitals sometimes used to explain phenomena with lanthanides. It is always good to check the yttrium result versus a late lanthanide when possible.

The isolation of $\{[(Me_3Si)_2N]_2Y(THF)\}_2(\mu\text{-}\eta^2\text{:}\eta^2\text{-}N_2)[Na(THF)_6]$, **8**, and $\{[(Me_3Si)_2N]_2Er(THF)\}_2(\mu\text{-}\eta^2\text{:}\eta^2\text{-}N_2)[Na(THF)_6]$, **9**, shows that the LnA_3/M method for forming $(N_2)^{3-}$ complexes is viable with Na as well as K. It was conceivable that the more reduced state of $(N_2)^{3-}$ versus $(N_2)^{2-}$ could only be reached with K (−2.9 V vs NHE) and not Na (−2.7 V vs NHE). The fact that $(N_2)^{3-}$ complexes could be made with Dy^{2+} in Scheme 1 (−2.5 V calculated vs NHE),[60] suggested that Na reduction should also be successful if these reactions follow the calculated general redox potentials of the metals. However, this latter trend must also always be checked.

The eight structurally characterized examples of the $(N_2)^{3-}$ complexes shown in Table 2 provide a consistent picture of the type of metrical parameters expected for this formerly unusual radical trianion. Similar parameters are observed with both amide and aryloxide ancillary ligands and with metals ranging in size from Dy^{3+} to Lu^{3+}. Although the variation in metal size is not yet great in this series, comparison of these data shows that amide and aryloxide compounds give similar parameters. The N−N distances do not depend on the outer sphere counterions, as expected, and they also are rather invariant when the alkali metal is attached as in **2b** and **4b**.

The interconversions of Ln_2N_2 and Ln_2N_2M complexes using excess KC_8 for reduction and Hg for oxidation are consistent with the chemistry expected for $(N_2)^{2-}$ and $(N_2)^{3-}$ complexes. However, the dependence on the method of combining reagents in determining the amounts of these compounds that can be isolated was surprising. Apparently, the balance between reaction pathways leading to $(N_2)^{2-}$ versus $(N_2)^{3-}$ is highly sensitive to concentration and KC_8 accessibility. The presence of metalation products, for example, $\{[(Me_3Si)_2N]_2Y[CH_2Si(Me_2)NSiMe_3]\}[K(THF)_2]$, **11**, and "ate" salts, LnA_4K, further complicates the reaction system. Considering that the KA byproduct of every LnA_3/K reaction could conceivably only form metalated products and react with LnA_3 starting material to make LnA_4K, it is remarkable that Ln_2N_2 and Ln_2N_2M products can be isolated at all!

The DFT analysis of $[(C_5Me_4H)_2Sc]_2(\mu\text{-}\eta^2\text{:}\eta^2\text{-}N_2)$, $\{[(Me_3Si)_2N]_2Y(THF)\}_2(\mu\text{-}\eta^2\text{:}\eta^2\text{-}N_2)$, **3**, $\{[(Me_3Si)_2N]_2Lu(THF)\}_2(\mu\text{-}\eta^2\text{:}\eta^2\text{-}N_2)$, **5**, and $[(ArO)_2Dy(THF)_2]_2(\mu\text{-}\eta^2\text{:}\eta^2\text{-}N_2)$, **1**, shows the bonding to be quite similar. In each case, it is the energy matching of nd orbitals with the π^* orbital of N_2 that makes the primary bond between the metals and the nitrogen. Net transfer of one valence electron per metal to the N_2 generates the $(N_2)^{2-}$ ion that is stabilized by this nd-π^* overlap. Although this is not unexpected for the 3d scandium and 4d yttrium ions, it also extends to the $4f^{14}$ Lu^{3+}. Since it is well-known that the limited radial extension of the 4f orbitals reduces their contribution to bonding, the use of the high-lying 5d orbitals becomes necessary. Contributions to bonding by the 5d have previously been invoked to explain the bonding in other lanthanide complexes.[63] It was uncertain if this trend of 5d contribution would persist beyond lutetium, which is the lanthanide closest to a transition metal in the periodic table. However, the calculation on $4f^9$ Dy^{3+} also shows that the 5d orbitals are the main contributors to the bonding in the reduced dinitrogen complexes. This scandium, yttrium, lutetium, and dysprosium series provides a good theoretical explanation for the similarity in structure and reactivity observed experimentally between these metals.

Conclusion

For the first time, aryloxide was successfully used as the anionic ligand in the LnA_3/M system to afford both the $(N_2)^{2-}$ and $(N_2)^{3-}$ reduced dinitrogen lanthanide complexes. The $(N_2)^{3-}$ complexes can be made with Lu^{3+}, La^{3+}, and Er^{3+} as well as Y^{3+} and Dy^{3+}. Sodium as well as potassium salts have been isolated and crystallographic data are now available on eight different examples. Facile methods are available to interconvert $(N_2)^{2-}$ and $(N_2)^{3-}$ complexes by reduction/oxidation using KC_8 and Hg, respectively. The isolation of $(N_2)^{3-}$ complexes can be enhanced by addition of 18-crown-6 to sequester the alkali metal counteraction and metalation byproducts have been identified. DFT calculations show a remarkable similarity in bonding in the $(N_2)^{2-}$ $\{[(Me_3Si)_2N]_2Ln(THF)\}_2(\mu\text{-}\eta^2\text{:}\eta^2\text{-}N_2)$ amide complexes of closed shell Y^{3+} and Lu^{3+}, the closed shell Sc^{3+} complex, $[(C_5Me_4H)_2Sc]_2(\mu\text{-}\eta^2\text{:}\eta^2\text{-}N_2)$, and the $(N_2)^{2-}$ aryloxide complex of open shell Dy^{3+}, $[(ArO)_2Dy(THF)_2]_2(\mu\text{-}\eta^2\text{:}\eta^2\text{-}N_2)$, as well as in the $(N_2)^{3-}$ complexes of Y^{3+}, Lu^{3+}, and Dy^{3+}. In each case nd orbital involvement is crucial in making the metal dinitrogen connection. Overall, the LnA_3/M dinitrogen reduction system is a rich

(59) Evans, W. J.; Allen, N. T.; Ziller, J. W. *J. Am. Chem. Soc.* **2000**, *122*, 11749.
(60) Morss, L. R. *Chem. Rev.* **1976**, *76*, 827.
(61) Arnold, P. L.; Liddle, S. T. *Organometallics* **2006**, *25*, 1485.
(62) Korobkov, I.; Gorelsky, S.; Gambarotta, S. *J. Am. Chem. Soc.* **2009**, *131*, 10406.
(63) Ortiz, J. V.; Hoffmann, R. *Inorg. Chem.* **1985**, *24*, 2095.

but complicated source of new chemistry for both lanthanides and dinitrogen.

Acknowledgment. We thank the U.S. National Science Foundation for support of this research through CHE-1010002, CHE-0723168, and CHE-0840513. We also thank the following people for experimental assistance: D. C. Lacy, Dr. E. Fadeev, Professors M. J. Nilges and A. S. Borovik (EPR), Dr. M. K. Takase (X-ray), Dr. P. R. Dennison (NMR), Dr. N. R. M. Crawford (computations), and T. J. Mueller (elemental analysis).

Supporting Information Available: X-ray data collection, structure solution, and refinement (PDF) and X-ray diffraction details of compounds **6**, **8**, **9**, **10**, and **12**. Additional DFT plots of compounds **2a** and **6**. This material is available free of charge via the Internet at http://pubs.acs.org.